IEEE Access
Multidisciplinary | Rapid Review | Open Access Journal

Received March 5, 2019, accepted March 18, 2019, date of publication March 29, 2019, date of current version April 15, 2019.

Digital Object Identifier 10.1109/ACCESS.2019.2908282

SAR Image Change Detection Based on Mathematical Morphology and the K-Means Clustering Algorithm

LUYANG LIU[1], ZHENHONG JIA[1], JIE YANG[2], AND NIKOLA K. KASABOV[3], (Fellow, IEEE)

[1]College of Information Science and Engineering, Xinjiang University, Urumqi 830046, China
[2]Institute of Image Processing and Pattern Recognition, Shanghai Jiao Tong University, Shanghai 200400, China
[3]Knowledge Engineering and Discovery Research Institute, Auckland University of Technology, Auckland 1020, New Zealand

Corresponding author: Zhenhong Jia (jzhh9009@sohu.com)

This work was supported in part by the International Cooperative Research and Personnel Training Projects of the Ministry of Education of the People's Republic of China, under Grant DICE2014-2029 and Grant 2016-2196.

ABSTRACT Synthetic aperture radar (SAR) images have been applied in disaster monitoring and environmental monitoring. With the objective of reducing the effect of noise on SAR image change detection, this paper presents an approach based on mathematical morphology filtering and K-means clustering for SAR image change detection. First, the multiplicative noise in two SAR images is transformed into additive noise by a logarithmic transformation. Second, the two multitemporal SAR images are denoised by morphological filtering. Third, the mean ratio operator and subtraction operator are used to obtain two difference images. Median filtering is applied to the difference image based on a simple combination of the two difference images. Since an accurate statistical model for the difference image cannot be easily established, the results of change detection are clustered using the K-means algorithm. A comparison of the experimental approach with other algorithms shows that the proposed algorithm can decrease the detection time and improve the detection result.

INDEX TERMS Image change detection, mathematical morphology filter, K-means clustering, logarithmic transformation, synthetic aperture radar (SAR) image.

I. INTRODUCTION

Remote sensing image change detection is a process in which changes in a geographical surface are determined by analyzing the images acquired at different times in the same geographical location [1]–[3]. Synthetic aperture radar (SAR) images are created by successive pulses of radio waves and echoes of each pulse. SAR images are usually used in remote sensing for landscape observation. Synthetic aperture radar (SAR) image change detection has become an important method with the development and application of remote sensing technology and because SAR can obtain image data under all illumination and weather conditions [4], [5]. The results of change detection can be improved by high-quality difference images. The subtraction operator can easily reflect the real change and the details of the area. However, the difference image obtained by the subtraction operator is easily influenced by noise. The speckle noise in SAR images reduces the quality of SAR image change detection. Many studies have focused on this topic. For example, Inglada proposed a mean ratio operator that can suppress the noise in image change detection [6], and the neighborhood-based ratio operator [7] proposed by Gong reduces the influence of noise and yields a high-quality difference image to improve the results of SAR image change detection. Celik used principal component analysis (PCA) to extract pixel features and then implemented a K-means clustering algorithm to obtain the change detection result. This method can suppress the speckle noise in SAR image change detection [8]. Li et al. denoised images based on the non-subsampled Contourlet transform and then used a fuzzy C-means (FCM) clustering algorithm to obtain the change detection results [9]. Gong et al. obtained the difference image by merging a mean ratio difference image and a logarithmic ratio difference image and then used fuzzy local information C-means (FLICM) clustering algorithm segmentation to obtain the change detection result. Compared to previously proposed methods, this approach reduces the noise and improves the accuracy of the change

The associate editor coordinating the review of this manuscript and approving it for publication was Kim-Kwang Raymond Choo.

detection result [10]. Yousif et al. used PCA and a non-local mean (NLM) algorithm to denoise SAR images for change detection [11]. In addition, spatial coding is widely used for such processes. Wang extracted pixel features from SAR images based on a spatial coding and pooling method. This method is robust to speckle noise; however, it requires more time than traditional methods to obtain the pixel features [5]. Wang used key points determined by scale-invariant feature transformation (SIFT) to reduce the detection range, and this approach is robust to speckle noise [12]. With the evolution of artificial intelligence, some artificial intelligence methods, such as deep learning [13] and dictionary learning [14] have also been successfully applied to SAR image detection. Furthermore, an SAR change detection algorithm that does not require labeled data was proposed by Shang et al [15]. The date label obtained by FCM is pre-classified, and the selected sample and self-step learning are used to train a classifier. The change detection result is obtained by the trained classifier. Some statistical techniques are also applied in SAR image change detection. It is important to build a suitable statistical model for SAR image change detection. The Gaussian distribution [16] and Markov random field [17] are commonly used in SAR image change detection. Some other distributions, such as the Gamma distribution [18], [19] and Wishart distribution [20], have also been successfully used in SAR image change detection. Saliency extraction has also recently been applied in change detection [21], [22]. After the registration of two SAR images, the two images still have considerable noise; thus, the real change detection result cannot be easily obtained from the registered SAR images. The accuracy of the change detection result can be improved in the transform domain, but this improvement increases the detection time due to the complexity of the operation. Obtaining the change detection result from the difference image is another important issue. Several traditional algorithms, such as the K-means clustering, Otsu, EM, FCM clustering, and FLICM algorithms, have been successfully applied for image change detection.

First, the multiplicative noise of the SAR image is transformed to additive noise by a logarithmic transformation. Compared to multiplicative noise, additive noise is easier to process. Second, the SAR images are denoised with a morphological filter. Third, the difference image is obtained based on a mean ratio operator and subtraction operator. Then, the final difference image is filtered by median filtering. Finally, the changed area is obtained by the K-means clustering algorithm. The simulation results show that the method not only improves the detection results but also decreases the detection time compared to that of traditional algorithms.

II. SAR IMAGE CHANGE DETECTION BASED ON MATHEMATICAL MORPHOLOGY AND THE K-MEANS ALGORITHM

Mathematical morphology is characterized by a simple structure and convenient calculations. The edges and details of the images obtained by morphology filters are well preserved. Mathematical morphology is widely used in image retrieval [23], satellite imaging [24], color image segmentation [25]–[27], image denoising [28], [29], and image fusion [30]. Change detection methods can be classified into supervised detection and unsupervised detection [31]. Although mathematical morphology is widely used in image processing, this study is the first time the approach has been used for SAR change detection. Unsupervised detection methods do not require prior knowledge. An unsupervised approach is applied in this paper. Let $X_1 = \{X_1(i,j) \mid 1 < i < H, 1 < i < W\}$ and $X_2 = \{X_2(i,j) \mid 1 < i < H, 1 < i < W\}$ be two calibrated SAR images. The two images have the same width W and the same height H. $\Omega = \{\omega_c, \omega_n\}$ represents the change detection result, where ω_c represents the changed pixels and ω_n represents the unchanged pixels. The algorithm flow chart shown in Figure 1 mainly consists of three steps: 1) perform a logarithmic transformation used to transform two SAR images; then, denoise the images using morphological filters; 2) combine the two difference images obtained by the mean ratio operator and subtraction operator; then, apply a median filter to the combined image to obtain the final difference image; and 3) use the K-means clustering algorithm, which does not require any distribution assumption, to find the changed area and unchanged area.

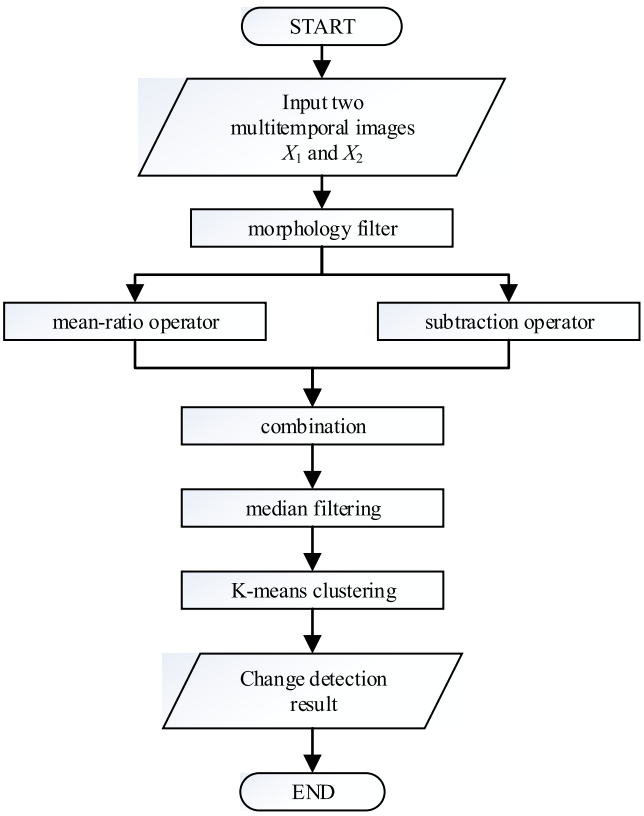

FIGURE 1. Algorithm flowchart.

A. MORPHOLOGICAL FILTER

The multiplicative noise in SAR images will affect the change detection results. When logarithmic transforms are performed, multiplicative noise is transformed to additive noise [32]. However, logarithmic transforms can enhance low-intensity pixels and compress pixel values [33]. After the registration of two SAR images X_1 and X_2, Im_1 and Im_2can be obtained by logarithmic transformation as follows:

$$Im_1(i,j) = log(X_1 + 1) \quad (1)$$

$$Im_2(i,j) = log(X_2 + 1) \quad (2)$$

where log represents the natural logarithm and $X_k + 1$ $(k = 1, 2)$ ensures that $X_k(k = 1, 2)$ is greater than 0 and makes $Im_k(i,j)(k = 1, 2)$ greater than or equal to 0. After the logarithmic transforms are implemented, the two images are linearly normalized to the range [0, 1].

Mathematical morphology operations include two sets in image processing: the image pixel set and the small set or image of structure elements (SEs). Dilation, erosion, opening, and closing are four basic operations in mathematical morphology [34]. Using a combination of dilation and erosion can yield all the morphological filters [35].

Let F represents a gray image and S represent the SEs.

The dilation operation is defined as follows.

$$F \oplus S(x,y) = \max_{(x',y')\epsilon s} \{F\left(x - x', y - y'\right) + S\left(x', y'\right)\} \quad (3)$$

The erosion operation is defined as follows.

$$F \Theta S(x,y) = \max_{(x',y')\epsilon s} \{F\left(x + x', y + y'\right) - S\left(x', y'\right)\} \quad (4)$$

Dilating an image is the same as finding the local maximum and will increase the highlighted area in the image.

Implementing dilation and erosion processes can obtain the open operation and close operation, which are defined as follows.

$$F \circ S = (F \Theta S) \oplus S \quad (5)$$

$$F \bullet S = (F \oplus S) \Theta S \quad (6)$$

The open operation is often used to remove small bright details that are smaller than SEs, and the close operation removes small dark details. Alternately, the open and close operations can be used to remove small noise components [36], [37]. The morphology filter is given as follows.

$$(F \bullet S) \circ S = \{[(F \oplus S) \Theta S]\} \oplus S \quad (7)$$

According to Equation (7), a new morphology filter can be obtained, as shown in Equations (8) and (9):

$$F_{1O} = MAX(MIN(F \bullet S_1, F \bullet S_2) \circ S_1, MIN(F \bullet S_1, F \bullet S_2) \circ S_2) \quad (8)$$

$$F_O = MAX(MIN(F_{1O} \bullet S_3, F \bullet S_4) \circ S_3, MIN(F_{1O} \bullet S_3, F \bullet S_4) \circ S_4) \quad (9)$$

where S_1, S_2, S_3, and S_4 are four SEs and F represents the SAR image. Notably, when S_1 and S_2 are the same, Equation (8) simplifies to Equation (7). In addition, this method primarily uses two-stage filtering. F_{1O} is the first stage result, and F_O is the final filtering result. *MAX* and *MIN* represent the maximum and minimum values of corresponding pixels in two images, respectively. First, the close operation with the two SEs removes the dark details from an image. To avoid losing too much detail of the open operation, we choose the minimum of the two results. To reduce the bright details in an image, the open operation is applied to the previous result based on the same two SEs. Because the open and close operations are dual operators, we chose the maximum of the open operation in this analysis. Similarly, the final result F_O is obtained via a similar method using two different SEs. To preserve more details, S_1 and S_2 are typically of small size. Moreover, some large components cannot be removed by the first stage of filtering. Therefore, for better performance, S_3 and S_4 should not be smaller than S_1 and S_2.

B. GENERATING THE DIFFERENCE IMAGE

After Im_1 and Im_2 are denoised by the morphology filter, images F_1 and F_2 are obtained. X_m and X_d are generated by the mean ratio operator and the subtraction operator as follows:

$$X_m(i,j) = 1 - min\left(\frac{u_1(i,j)}{u_2(i,j)}, \frac{u_2(i,j)}{u_1(i,j)}\right) \quad (10)$$

$$X_d(i,j) = |F_1(i,j) - F_2(i,j)| \quad (11)$$

where $u_1(i,j)$ and $u_2(i,j)$ are the mean values of all pixels in a 3×3 neighborhood of pixel (i, j) in F_1 and F_2, respectively.

The subtraction operator is consistent with the real change in the results for a given region, but the results are easily affected by noise. The mean ratio operator can suppress the noise in images, but the image obtained from the mean ratio operator will be ambiguous. To effectively utilize the advantages of the two types of difference images and improve the detection results [38], a final difference image D is defined by the following formula:

$$D = \alpha X_m + (1 - \alpha) X_d \quad (12)$$

where $\alpha \geq 0$. For different images, the parameter α can be adjusted to balance the effect of noise; this method can yield better detection results than a single method.

C. K-MEANS CLUSTERING ALGORITHM

As a classic unsupervised classification algorithm, K-means clustering is based on a set of k centroids for each class and minimizing the variance within k category classes [39]. Let CD be the result of change detection. In addition, c_i and c_d represent the centroids of the changed pixels and unchanged pixels, respectively. When $k = 2$, the K-means++ algorithm is used to select the initial value [40]. Compared with the K-means algorithm for randomly selecting the initial centroids, the K-means++ algorithm can obtain the initial centroids for better clustering results. For n samples, K-means++ algorithm first randomly selects a

centroid $C = \{c_1\}$. Then the maximum probability is calculated by (13)čž

$$p = \arg\min_{x} \frac{d(x, C)^2}{\sum_{j=1,\ldots,n} d(x_j, C)^2} \tag{13}$$

where $d(x, C)$ as shown in (14) represents the shortest distance between a sample and the centroid.

$$d\,(x, C) = \sum\nolimits_{m=1,\ldots,k} \|x - c_m\|_2^2 \tag{14}$$

take the next centroid:

$$C = C \cup \{p\} \tag{15}$$

until we have taken k centroids.

The pixels are of the 255 gray level in the changed class set and the 0 gray level in the unchanged class set. The associated process is as follows.

$$CD(i,j) = \begin{cases} 255 & \|D(i,j) - c_i\|_2^2 \le \|D(i,j) - c_d\|_2^2 \\ 0 & others \end{cases} \tag{16}$$

III. EXPERIMENTAL ANALYSIS

A. DESCRIPTION OF THE EXPERIMENTAL DATA

The first SAR images shown in Figure 2a and 2b are of a region in Ottawa, Canada. The images are 290 × 350 pixels in size and were obtained in May 1997 and August 1997. The cause of the change is the start of the rainy season, as shown in Figure 2c.

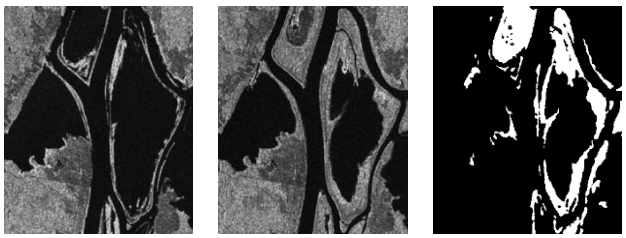

FIGURE 2. Ottawa data set: (a) May 1997; (b) August 1997; (c) The reference detected change image.

The second set of SAR images is from Bern, Switzerland, and they are 301 × 301 pixels in size, as shown in Figure 3a and 3b. The images were recorded in April 1999 and May 1999. The main reason for the change in the two images is flooding, as shown in Figure 3c.

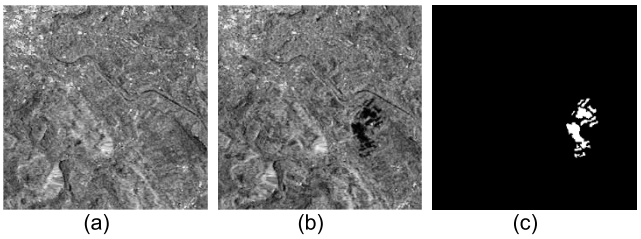

FIGURE 3. Bern data set: (a) April 1999; (b) May 1999; (c) The reference detected change image.

The third set of SAR images is from Shimen Reservoir in Taoyuan County, Daxi Town, northern Taiwan, as shown in Figure 4a and Figure 4b. The images were captured by the ERS-2 satellite on October 24, 1998, and September 4, 1999. The remote sensing images are both 500 × 500 pixels in size and have a 256 gray level. The reference image is shown in Figure 4c. The reference image obtained by manual analysis shows the real change between the two images taken at different times. In the reference image, the changed pixels are shown in white, and the unchanged pixels are shown in black.

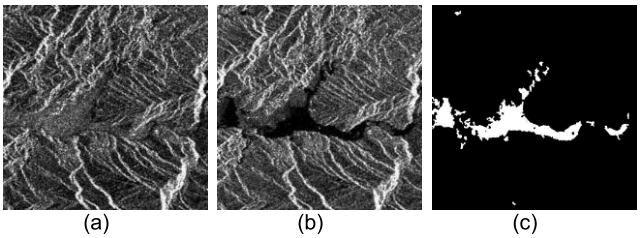

FIGURE 4. Shimen data set: (a) October 24, 1998; (b)September 4, 1999; (c) The reference detected change image.

B. ANALYSIS OF THE RESULTS

In order to validate the performance of the proposed method, the proposed method and other four methods are applied in three data sets and the objective indicators are presented. The experimental environment used in the above three experiments includes an Intel Core i5-6500@3.20 GHz processor with 4 GB of memory, and the software used was MATLAB2016 (64 bit). The objective indicators adopted are false negatives (FN), false positives (FP), the overall error (OE), the percentage correct classification (PCC), the Kappa coefficient and the run time (T) [41]. Choosing a proper structural element is important for the change detection result. Small structural elements preserve detail but are susceptible to noise. Large structural elements blur details while removing noise. In general, it is appropriate to choose a linear structure. The size of the structural element should be larger than the size of the noise image but smaller than the size of the non-noise image. As show in Figure 7-9d, there are many small white misdetected areas that can be considered to be caused by noise. Referring to Figure 7-9d, we select the following size and angle of the structural elements. For the first set of data, S_1 is chosen to be a linear structure element with a length of 2 and an angle of 0°; S_2 is chosen to be a linear structure element with a length of 2 and an angle of 90°; S_3 is chosen to be a linear structural element with a length of 3 and an angle of 0°; S_4 is chosen to be linear structural element with a length of 3 and an angle of 90°. For the second set of data $S_1$is chosen to be a linear structural element with a length of 2 and an angle of -45°; S_2 is chosen to be a linear structural element with a length of 2 and an angle of -30°; S_3 is chosen to be a linear structural element with a length of 2 and an angle of 45°; S_4 is chosen to be a linear structural element with a length of 2 and an angle of 30°. For the third

set of data, S_1 and S_2 are chosen to be 5×5 square structural elements; S_3 is chosen to be a linear structural element with a length of 5 and an angle of 0°; S_4 is chosen to be a linear structural element with a length of 5 and an angle of 90°.

Figure 5 shows the results of different operators. Notably, the logarithmic transform enhances the low-intensity pixels and compresses the noise. Figure 5(c) and (d) show the results of the morphological filter. The details of the image are well preserved while small noise components are removed. The median filter is applied before clustering. The median filter can remove the isolated pixels and effectively preserve the edges.

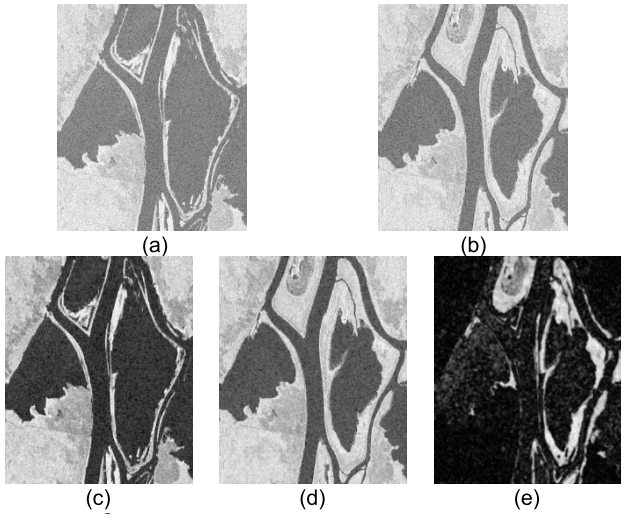

FIGURE 5. Steps in generating a difference image: (a) Image at time t_1 obtained by logarithmic transforms; (b) Image at time t_2 obtained by logarithmic transforms; (c) Image at time t_1 obtained by a morphological filter; (d) Image at time t_2 obtained by a morphological filter; (e) Image obtained by a median filter.

The relationship between the performance and α is shown in Figure 6. The performance of α is shown by presenting PCC and Kappa coefficient values for the three data sets. The range of α is 0 to 1.5, and the interval is 0.1. For different α, there are corresponding PCC and Kappa coefficient. From figure 6, when α is approximately 1, the maximum value of PCC and Kappa coefficient obtained. To obtain better performance, the value of α is set to approximately 1 for the three data sets. Compared to the subtraction difference image, there is relatively little noise in the mean ratio difference image. When α is 0, only the subtraction difference image is used. Figure 6 shows that the performances of Kappa and PCC are lowest. The PCC and Kappa values of the three data sets are not reliable after $\alpha > 1.5$. As α changes, different results are obtained. Specifically, as α approaches 1, the performances improve. Figure 6 clearly shows that when the values of the three sets of data α are 1.1, 0.8, 1, the PCC and Kappa reach maximum values. Thus, a suitable parameter α can improve the detection results.

To demonstrate the effectiveness of the proposed algorithm, it is compared with the DWT-FLICM [41], PCA-K-means [42], TV-K-means [43], and PCAnet [44]

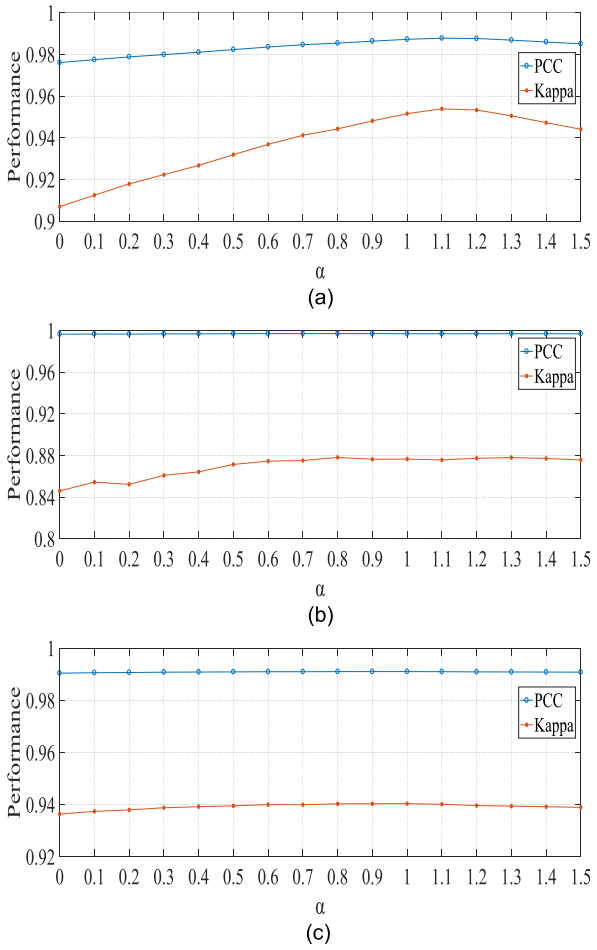

FIGURE 6. Performance of the proposed algorithm against the parameter α. a) Ottawa data set; (b) Bern data set; (c) Shimen data set.

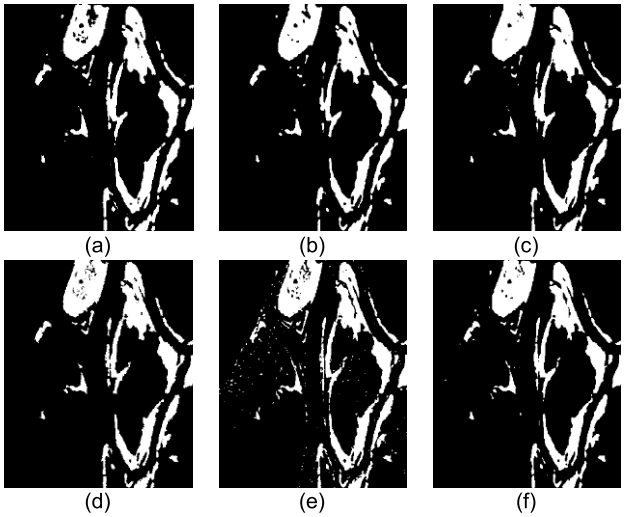

FIGURE 7. Results of SAR image change detection for the Ottawa data set: (a) PCA-K-means; (b) DWT-FLICM; (c) TV-K-means; (d) PCAnet; (e) RM; (f) Proposed.

algorithms, and the algorithm uses only one difference image and removes the proposed denoising and combination step (RM). Figure 7 to Figure 9, we can see that the RM

TABLE 1. Performance measures for the Ottawa dataset.

Data set	Method	FN	FP	OE	PCC (%)	Kappa	$\overline{T}$(s)
Ottawa	DWT-FLICM	1654	163	1817	98.21	0.9301	6.04
	PCA-K-means	1529	979	2508	97.52	0.9062	8.74
	TV-K-means	1382	714	2096	97.93	0.9214	5.87
	PCAnet	750	1088	1838	98.19	0.9313	2010.23
	RM(α=0)	247	2603	2850	97.19	0.8989	**1.86**
	Proposed(α=1.1)	879	374	1253	**98.77**	**0.9532**	2.35

TABLE 2. Performance measures for the Bern dataset.

Data set	Method	FN	FP	OE	PCC (%)	Kappa	$\overline{T}$(s)
Bern	DWT-FLICM	175	154	329	99.64	0.8570	5.78
	PCA-K-means	162	119	281	99.69	0.8745	8.47
	TV-K-means	133	157	290	99.68	0.8741	3.10
	PCAnet	27	477	504	99.44	0.7264	1401.97
	RM(α=0)	281	296	577	99.36	0.7034	**1.76**
	Proposed(α=0.8)	157	116	273	**99.70**	**0.8782**	2.04

TABLE 3. Performance measures for the Shimen dataset.

Data set	Method	FN	FP	OE	PCC (%)	Kappa	$\overline{T}$(s)
Shimen	DWT-FLICM	1796	802	2598	98.96	0.9325	13.01
	PCA-K-means	2708	33	2741	98.90	0.9261	20.74
	TV-K-means	2310	202	2512	98.99	0.9331	18.42
	PCAnet	3659	87	3746	98.50	0.8956	3508.86
	RM(α=0)	2173	3975	6148	97.54	0.8493	**2.62**
	Proposed(α=1)	2136	107	2272	**99.10**	**0.9404**	3.98

TABLE 4. Complexity of each process.

Process	Complexity	Process	Complexity
Logarithmic transformation	O(n)	Median filtering	O(nr_m^2logr)
DI generation	O(r_d^2n)	K-means clustering	O(kndt)
Mathematical Morphology process	O(wn)	Proposed algorithm	O(kndt)

algorithm is greatly affected by noise. For the Ottawa data set, Figure 7, shows that the image produced by the proposed method is closer to the reference image and preserves more details than the images produced by the other algorithms. Figure 7(b) and (c) show that DWT-FLICM and TV-K-means reduce the noise but lose the detail in changed areas. Table 1 shows that compared with the other algorithms, the proposed method exhibits better performance based on the OE, PCC, and Kappa coefficient and requires less time. The analysis of the Bern data set in Table 2 indicates that the PCC and Kappa coefficient of the proposed method are superior to those of the other algorithms. Compared to the other algorithms, the time required to run the proposed algorithm is reduced by a factor of 1.06 to 1399.93 seconds. As shown in Figure 8, the DWT-FLICM algorithm removes the noise but loses the details. The TV-K-means algorithm preserves details, but Kappa and OE are smaller compared with our proposed algorithm. As for PCAnet, many of the change pixels are not detected, and a long time is required to obtain the change detection result. For the Shimen data set, as shown in Figure 9, there are few false detection areas with the proposed algorithm. Compared to the other five algorithms,

TABLE 5. Average performance measures for the SAR images.

Method	$\overline{\text{FN}}$ (%)	$\overline{\text{FP}}$ (%)	$\overline{\text{OE}}$ (%)	$\overline{\text{PCC}}$ (%)	$\overline{\text{Kappa}}$	$\overline{\text{T}}$ (s)
DWT-FLICM	1.14	1.58	2.72	97.28	0.8228	8.66
PCA-K-means	1.15	2.66	3.81	96.19	0.7993	17.28
TV-K-means	0.52	2.60	3.12	96.88	0.8045	13.64
PCAnet	8.13	1.11	9.24	90.76	0.6006	2294.65
RM	1.47	6.41	7.88	92.12	0.6949	**2.31**
Proposed	0.59	1.23	1.82	**98.18**	**0.8708**	2.98

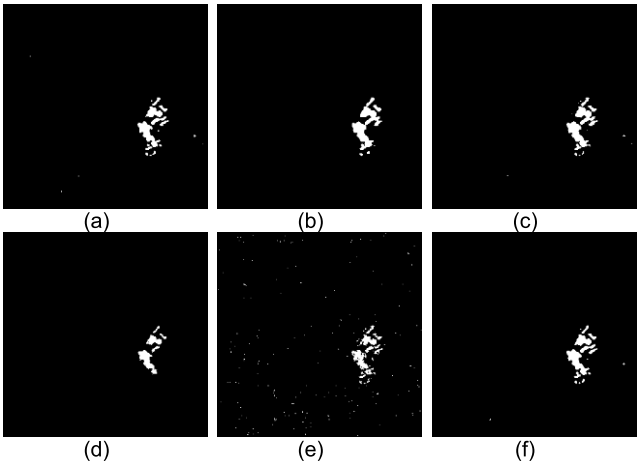

FIGURE 8. Results of SAR image change detection for the Bern data set: (a) PCA-K-means; (b) DWT-FLICM; (c) TV-K-means; (d) PCAnet; (e) RM; (f) Proposed.

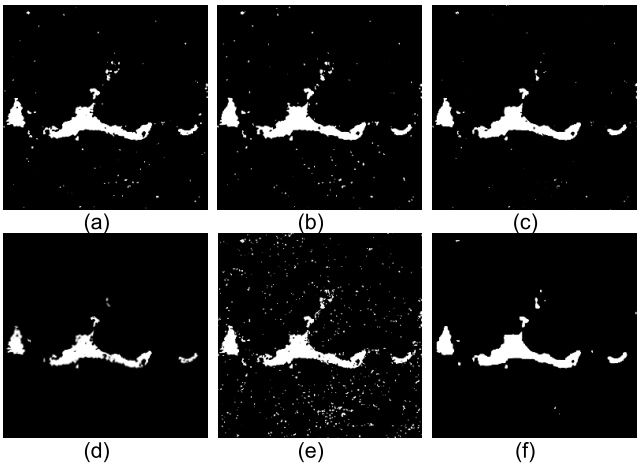

FIGURE 9. Results of SAR image change detection for the Shimen data set: (a) PCA-K-means; (b) DWT-FLICM; (c) TV-K-means; (d) PCAnet; (e) RM; (f) Proposed.

the proposed algorithm preserves more details and removes more noise. Table 3 illustrates that the time required for the proposed method is the shortest and that the PCC and Kappa values are the highest. The time required for PCAnet is 882 times that of the proposed algorithm. When the size of the SAR image increases, the time requirement of each algorithm also increases. As presented in Table 1 and Table 3, as the image size increased, the time required to run the proposed algorithm increased by 69% compared to 118%, 137%, 241% and 74.6% for the DWT-FLICM, PCA-K-means, TV-K-means and PCAnet algorithms, respectively. Therefore, the time increase was smallest for the proposed algorithm. Specifically, because the results of the proposed method are within the logarithmic domain and are based on a simple framework, the detection time is reduced.

Table 4 shows the complexity of each step of the proposed algorithm. From Figure 1 and section II, there are five steps: logarithmic transformation, DI generation, mathematical morphology process, median filtering, and K-means clustering. The complexity of the proposed algorithm consists of the five steps. n represents the total number of pixels of the image. The window sizes of the mean ratio operator and median filtering are represented by r_d and r_m. w is the number of pixels in the largest structural element. k represents the number of cluster centers and is set to 2. d is the distance calculation complexity. The k-means iteration is represented by t.

Because r_d, r_m and w are much smaller than dt, as shown in Table 4, the complexity of the proposed algorithm is O(kndt).

C. ANALYSIS OF THE AVERAGE EXPERIMENTAL RESULTS

The 20 sets of SAR image data were used for testing, and the average results were calculated for the five algorithms discussed in the previous section. Each of the 20 sets of SAR images includes two images taken at different times and a manually analyzed reference detected change area image. The average results of each algorithm are shown in Table 5.

The test of each group of data was run 10 times to obtain the average change detection result, as shown in Table 5. These average results show that compared with the other four methods, adjusting the parameters of the proposed algorithm can yield the most accurate test results. The proposed method outperforms the DWT-FLICM, TV-K-means, PCA-K-means and PCAnet algorithms in terms of the detection time.

IV. CONCLUSIONS

In this paper, we present a morphological filtering method for SAR image change detection. SAR change detection has many applications, such as geographical surface changes

caused by floods. This algorithm can be applied to large SAR image change detection with less time consumption. We perform morphological filtering based on SAR images that are logarithmically transformed and then obtain the two difference images using the mean ratio operator and subtraction operator. After combining the two difference images, the final difference image is obtained through median filtering. Finally, the initial cluster centers are initialized by the K-means++ algorithm, and K-means clustering is used to extract the change area from the image. Using both the mean ratio operator and subtraction operator in the logarithmic domain improves the change detection results. The algorithm processes images in the logarithmic domain and reduces the computational time. The results of the experiment suggest that the proposed algorithm detects the actual change and has a shorter detection time than previous algorithms. Further improvements will be obtained in future work. In this paper, the structural elements and α are manually selected based on experience for different scenarios. We will consider using automatic morphological methods to extract features for unsupervised SAR image change detection to improve the accuracy of the change detection results.

REFERENCES

[1] R. J. Radke, S. Andra, O. Al-Kofahi, and B. Roysam, "Image change detection algorithms: A systematic survey," *IEEE Trans. Image Process.*, vol. 14, no. 3, pp. 294–307, Mar. 2005.

[2] P. Chen, Y. Zhang, Z. Jia, J. Yang, and N. Kasabov, "Remote sensing image change detection based on NSCT-HMT model and its application," *Sensors*, vol. 17, p. 1295, Jun. 2017.

[3] M. Jia and L. Wang, "Novel class-relativity non-local means with principal component analysis for multitemporal SAR image change detection," *Int. J. Remote Sens.*, vol. 39, no. 4, pp. 1068–1091, 2018.

[4] B. Hou, Q. Wei, Y. Zheng, and S. Wang, "Unsupervised change detection in SAR image based on gauss-log ratio image fusion and compressed projection," *IEEE J. Sel. Topics Appl. Earth Observ. Remote Sens.*, vol. 7, no. 8, pp. 3297–3317, Aug. 2014.

[5] S. Wang, L. Jiao, and S. Yang, "SAR images change detection based on spatial coding and nonlocal similarity pooling," *IEEE J. Sel. Topics Appl. Earth Observ. Remote Sens.*, vol. 9, no. 8, pp. 3452–3466, Aug. 2016.

[6] J. Inglada and G. Mercier, "A new statistical similarity measure for change detection in multitemporal SAR images and its extension to multiscale change analysis," *IEEE Trans. Geosci. Remote Sens.*, vol. 45, no. 5, pp. 1432–1445, May 2007.

[7] M. Gong, Y. Cao, and Q. Wu, "A neighborhood-based ratio approach for change detection in SAR images," *IEEE Geosci. Remote Sens. Lett.*, vol. 9, no. 2, pp. 307–311, Mar. 2012.

[8] T. Celik, "Unsupervised change detection in satellite images using principal component analysis and k-means clustering," *IEEE Geosci. Remote Sens. Lett.*, vol. 6, no. 4, pp. 772–776, Oct. 2009.

[9] L. Qingsong, Q. Xizhong, and J. Zhenhong, "An unsupervised change detection of SAR images based on NSCT and FCM clustering," *Laser J.*, vol. 34, no. 4, pp. 21–22, 2013.

[10] M. Gong, Z. Zhou, and J. Ma, "Change detection in synthetic aperture radar images based on image fusion and fuzzy clustering," *IEEE Trans. Image Process.*, vol. 21, no. 4, pp. 2141–2151, Apr. 2012.

[11] O. Yousif and Y. Ban, "Improving urban change detection from multitemporal SAR images using PCA-NLM," *IEEE Trans. Geosci. Remote Sens.*, vol. 51, no. 4, pp. 2032–2041, Apr. 2013.

[12] Y. Wang, L. Du, and H. Dai, "Unsupervised SAR image change detection based on SIFT keypoints and region information," *IEEE Geosci. Remote Sens. Lett.*, vol. 13, no. 7, pp. 931–935, Jul. 2016.

[13] N. Lv, C. Chen, T. Qiu, and A. K. Sangaiah, "Deep learning and superpixel feature extraction based on contractive autoencoder for change detection in SAR images," *IEEE Trans. Ind. Informat.*, vol. 14, no. 12, pp. 5530–5538, Dec. 2018.

[14] L. Li *et al.*, "Deformable dictionary learning for SAR image change detection," *IEEE Trans. Geosci. Remote Sens.*, vol. 56, no. 8, pp. 4605–4617, Aug. 2018.

[15] R. Shang, Y. Yuan, L. Jiao, M. Yang, and A. M. Ghalamzan, "A self-paced learning algorithm for change detection in synthetic aperture radar images?" *Signal Process.*, vol. 142, pp. 375–387, Jan. 2017.

[16] Y. Bazi, L. Bruzzone, and F. Melgani, "An unsupervised approach based on the generalized Gaussian model to automatic change detection in multitemporal SAR images," *IEEE Trans. Geosci. Remote Sens.*, vol. 43, no. 4, pp. 874–887, Apr. 2005.

[17] S. Martinis, A. Twele, and S. Voigt, "Unsupervised extraction of flood-induced backscatter changes in SAR data using Markov image modeling on irregular graphs," *IEEE Trans. Geosci. Remote Sens.*, vol. 49, no. 1, pp. 251–263, Jan. 2011.

[18] F. Crismer, G. Moser, V. A. Krylov, and S. B. Serpico, "Unsupervised change detection on synthetic aperture radar images with generalized gamma distribution," in *Proc. IEEE Int. Geosci. Remote Sens. Symp. (IGARSS)*, Jul. 2016, pp. 3350–3353.

[19] V. T. Vu, N. R. Gomes, M. I. Pettersson, P. Dammert, and H. Hellsten, "Bivariate gamma distribution for wavelength-resolution SAR change detection," *IEEE Trans. Geosci. Remote Sens.*, vol. 57, no. 1, pp. 473–481, Jan. 2018.

[20] W. Yang, X. Yang, T. Yan, H. Song, and G. S. Xia, "Region-based change detection for polarimetric SAR images using Wishart mixture models," *IEEE Trans. Geosci. Remote Sens.*, vol. 54, no. 11, pp. 6746–6756, Nov. 2016.

[21] Y. Zheng, L. Jiao, H. Liu, X. Zhang, B. Hou, and S. Wang, "Unsupervised saliency-guided SAR image change detection," *Pattern Recognit.*, vol. 61, pp. 309–326, Jan. 2017.

[22] Y. Zhang, S. Wang, C. Wang, J. Li, and H. Zhang, "SAR image change detection using saliency extraction and shearlet transform," *IEEE J. Sel. Topics Appl. Earth Observ. Remote Sens.*, vol. 11, no. 12, pp. 4701–4710, Dec. 2018.

[23] E. Aptoula, "Remote sensing image retrieval with global morphological texture descriptors," *IEEE Trans. Geosci. Remote Sens.*, vol. 52, no. 5, pp. 3023–3034, May 2014.

[24] Z. Wang, L. Du, and H. Su, "Target detection via Bayesian-morphological saliency in high-resolution SAR images," *IEEE Trans. Geosci. Remote Sens.*, vol. 55, no. 10, pp. 5455–5466, Oct. 2017.

[25] C. Meurie, O. Lezoray, L. Khoudour, and A. Elmoataz, "Morphological hierarchical segmentation and color spaces," *Int. J. Imag. Syst. Technol.*, vol. 20, no. 2, pp. 167–178, 2010.

[26] H.-C. Shih and E.-R. Liu, "Automatic reference color selection for adaptive mathematical morphology and application in image segmentation," *IEEE Trans. Image Process.*, vol. 25, no. 10, pp. 4665–4676, Oct. 2016.

[27] M. Koosha, K. Hajsadeghi, and M. Koosha, "Fine logarithmic adaptive soft morphological algorithm for synthetic aperture radar image segmentation," *IET Image Process.*, vol. 8, no. 2, pp. 90–102, Feb. 2014.

[28] T. Lei and Y.-Y. Fan, "Noise gradient reduction based on morphological dual operators," *IET Image Process.*, vol. 5, no. 1, pp. 1–17, 2011.

[29] P.-H. Lin, B.-H. Chen, F.-C. Cheng, and S.-C. Huang, "A morphological mean filter for impulse noise removal," *J. Display Technol.*, vol. 12, no. 4, pp. 344–350, Apr. 2016.

[30] X. Li, L. Wang, J. Wang, and X. Zhang, "Multi-focus image fusion algorithm based on multilevel morphological component analysis and support vector machine," *IET Image Process.*, vol. 11, no. 10, pp. 919–926, 2017.

[31] L. Jia, M. Li, P. Zhang, and Y. Wu, "SAR image change detection based on correlation kernel and multistage extreme learning machine," *IEEE Trans. Geosci. Remote Sens.*, vol. 54, no. 10, pp. 5993–6006, Oct. 2016.

[32] B. Xu, Y. Cui, Z. Li, B. Zuo, J. Yang, and J. Song, "Patch ordering-based SAR image despeckling via transform-domain filtering," *IEEE J. Sel. Topics Appl. Earth Observ. Remote Sens.*, vol. 8, no. 4, pp. 1682–1695, Apr. 2014.

[33] M. N. Sumaiya and R. S. S. Kumari, "Logarithmic mean-based thresholding for SAR image change detection," *IEEE Geosci. Remote Sens. Lett.*, vol. 13, no. 11, pp. 1726–1728, Nov. 2016.

[34] W. Huang, R. Wang, Y. Zhou, and X. Chen, "Simultaneous coherent and random noise attenuation by morphological filtering with dual-directional structuring element," *IEEE Geosci. Remote Sens. Lett.*, vol. 14, no. 10, pp. 1720–1724, Oct. 2017.

[35] F. G. B. De Natale and G. Boato, "Detecting morphological filtering of binary images," *IEEE Trans. Inf. Forensics Security*, vol. 12, no. 5, pp. 1207–1217, May 2017.
[36] D. Ze-Feng, Y. Zhou-Ping, and X. You-Lun, "High probability impulse noise-removing algorithm based on mathematical morphology," *IEEE Signal Process. Lett.*, vol. 14, no. 1, pp. 31–34, Jan. 2006.
[37] L. Hu, C. Qi, S. Chen, and Q. Wang, "An improved heuristic optimization algorithm for feature learning based on morphological filtering and its application," *IEEE Access*, vol. 6, pp. 22754–22763, 2018.
[38] Y. Zheng, X. Zhang, B. Hou, and G. Liu, "Using combined difference image and *k*-means clustering for SAR image change detection," *IEEE Geosci. Remote Sens. Lett.*, vol. 11, no. 3, pp. 691–695, Mar. 2014.
[39] R. M. Esteves, T. Hacker, and C. Rong, "Competitive k-means, a new accurate and distributed k-means algorithm for large datasets," in *Proc. IEEE 5th Int. Conf. Cloud Comput. Technol. Sci. (CloudCom)*, Dec. 2013, pp. 17–24.
[40] D. Arthur and S. Vassilvitskii, "k-means++: The advantages of careful seeding," in *Proc. 18th ACM-SIAM Symp. Discrete Algorithms*, 2007, pp. 1027–1035.
[41] J. Ma, M. Gong, and Z. Zhou, "Wavelet fusion on ratio images for change detection in SAR images," *IEEE Geosci. Remote Sens. Lett.*, vol. 9, no. 6, pp. 1122–1126, Nov. 2012.
[42] Y.-Q. Cheng, H.-C. Li, T. Celik, and F. Zhang, "FRFT-based improved algorithm of unsupervised change detection in SAR images via PCA and K-means clustering," in *Proc. Geosci. Remote Sens. Symp.*, 2014, pp. 1952–1955.
[43] X. Wang, Z. Jia, J. Yang, and N. Kasabov, "Change detection in SAR images based on the logarithmic transformation and total variation denoising method," *Remote Sens. Lett.*, vol. 8, no. 3, pp. 214–223, 2017.
[44] F. Gao, J. Dong, B. Li, and Q. Xu, "Automatic change detection in synthetic aperture radar images based on PCANet," *IEEE Geosci. Remote Sens. Lett.*, vol. 13, no. 12, pp. 1792–1796, Dec. 2016.

LUYANG LIU received the B.S. degrees from Central South University, Changsha, China, in 2010 and 2014, respectively. He is currently pursuing the M.S. degree with the Department of Information Science and Engineering, Xinjiang University, Urumqi, China. His research interest is in the area of image change detection image processing.

ZHENHONG JIA received the B.S. degree from Beijing Normal University, Beijing, China, in 1985, and the M.S. and Ph.D. degrees from Shanghai Jiao Tong University, Shanghai, China, in 1987 and 1995, respectively. He is currently a Professor with the Autonomous University Key Laboratory of Signal and Information Processing Laboratory, Xinjiang University, China. His research interests include digital image processing and optical information detection.

JIE YANG received the B.S. degrees from Shanghai Jiao Tong University, Shanghai, China, in 1982 and 1985, respectively, and the Ph.D. degree from the Department of Computer Science, Hamburg University, Hamburg, Germany, in 1994. He is currently a Professor with the Institute of Image Processing and Pattern Recognition, Shanghai Jiao Tong University. His major research interests are object detection and recognition, data fusion and data mining, and medical image processing.

NIKOLA K. KASABOV (M'93–SM'98–F'10) received the M.S. degree in computing and electrical engineering and the Ph.D. degree in mathematical sciences from the Technical University of Sofia, Sofia, Bulgaria, in 1971 and 1975, respectively. He is currently the Director and the Founder of the Knowledge Engineering and Discovery Research Institute, and a Professor of knowledge engineering with the School of Computing and Mathematical Sciences, Auckland University of Technology, Auckland, New Zealand. His major research interests are information science, computational intelligence, neural networks, bioinformatics, and neuroinformatics.